Concentration-Induced Conformational Change in Linear Polymer Threaded into Cyclic Molecules

Koichi Mayumi,*,† Noboru Osaka,‡ Hitoshi Endo,‡ Hideaki Yokoyama,† Yasuhiro Sakai,† Mitsuhiro Shibayama,‡ and Kohzo Ito*,†

Graduate School of Frontier Sciences, The University of Tokyo, 5-1-5 Kashiwanoha, Kashiwa, Chiba 277-8561, Japan, and Institute for Solid State Physics, The University of Tokyo, 5-1-5 Kashiwanoha, Kashiwa, Chiba 277-8581, Japan

Received May 6, 2008; Revised Manuscript Received July 2, 2008

ABSTRACT: The concentration-induced conformational change in hydroxypropylated polyrotaxane (H-PR) composed of poly(ethylene glycol) (PEG) and hydroxypropylated α-cyclodextrins (CDs) was investigated at various concentrations from the overlap concentration c^* to the semidilute regime by using the small-angle neutron scattering technique. We employed the generalized Zimm plot with the wormlike chain model to analyze the scattering functions of H-PR since they deviated from the Ornstein−Zernike equation particularly in the high-Q range. It was found that the persistence length of H-PR decreased with increasing polymer concentration c_p, while those of PEG remained unchanged in the same molar concentration regime. This unusual concentration dependence of polymer conformation for H-PR may indicate that CDs in H-PR could slide freely and rapidly over the whole range of PEG chains in the neighborhood of c^*, but their mobility was suppressed as c_p increased due to some molecular interaction among CDs.

1. Introduction

Supramolecules with topologically interlocked structures have attracted a great interest[1−3] because they have the degree of freedom of movement with topological restrictions. A typical example is provided by polyrotaxane (PR) in which a number of cyclic molecules are threaded onto a linear polymer and are trapped by capping the chain with bulky end groups.[2−9] The cyclic molecules in PR can slide and rotate on the polymer chain. The unique structure and dynamics of PR enable the application of various molecular devices in nanoscale: molecular tubes,[10] insulated molecular wires,[11,12] molecular shuttles,[3] drug delivery systems,[13] and multivalent ligand systems.[14] Recently, PR consisting of poly(ethylene glycol) (PEG) as a linear axis polymer and α-cyclodextrin (CD) as a cyclic molecule has been applied to producing a novel kind of gel called "slide-ring (SR) gel" by cross-linking CDs on different PRs.[15] SR gels demonstrate remarkable properties such as high extensibility and a great degree of swelling.[15,16] These macroscopic features of SR gels are derived from the nanoscale sliding motion of cyclic molecules: double-looped cross-links can move along polymer chains to minimize the local strain in the network just like pulleys. In order to confirm this pulley effect, the static structure of the SR gels under uniaxial deformation has been investigated by using the small-angle neutron scattering (SANS) and X-ray scattering (SAXS) techniques.[17−19] The results indicate that the spatial inhomogeneities in SR gels do not increase by stretching due to the pulley effect, while chemical gels increase the inhomogeneities by stretching.

In order to develop these unique materials made from PR and elucidate their properties, it is important to understand the dynamics and structure of PR in solution. The dynamic behavior of PR has been investigated by using the nuclear magnetic resonance spectroscopy (NMR)[20,21] and dynamic light scattering (DLS) technique.[22] DLS probes the concentration fluctuation that originates from the sliding motion of CDs in a semidilute solution. On the other hand, the static structure of PR has been observed using the SANS measurement.[23−25] The single-chain conformation of PR in a dilute solution changes with the number of CDs threaded on the PEG chains.[24] As the number of CDs increases, the PEG chain extends and the conformation changes from a Gaussian chain to a rodlike structure. In the semidilute regime, the scattering function for PR in deuterated dimethyl sulfoxide (DMSO-d_6) cannot be described by a Lorentz-type function, which is used to analyze the scattering functions of the usual polymers in semidilute solutions.[23]

In this work, we investigate the concentration dependence of the conformation of PR by using SANS, in comparison with the structure of the template PEG chain in the same molar concentration range. Recently, the generalized Zimm plot[26] allowed us to obtain detailed information on the conformation of a single polymer chain in the semidilute regime. In this study, we have attempted to apply this new analysis method to the scattering function of PR. We use hydroxypropylated polyrotaxane (H-PR) composed of PEG and hydroxypropylated α-cyclodextrins instead of PR without any modifications. The hydroxypropylation of PR weakens the hydrogen bonds between CDs and disperses CDs on the PEG chain, which considerably improves the solubility of PR in solutions, especially in an aqueous solution.[27,28]

2. Experimental Section

2.1. Materials. Poly(ethylene glycol) (PEG) was purchased from Fluka. The weight-average molecular weight of PEG was 3.5×10^4, and the polydispersity was 1.1. Polyrotaxane (PR), consisting of PEG, α-cyclodextrin (CD), and adamantanamine, was prepared by a previously reported method.[29] The average number of CDs per chain was determined to be 100 by ^{1}H NMR analysis, corresponding to 26% coverage of the PEG chains with CDs, assuming that a CD molecule can cover two PEG monomer units.[30] Some hydroxyl groups on the CD molecules were substituted by hydroxypropyl groups by using propylene oxide.[27,28] The average number of hydroxypropyl groups per CD molecule was determined to be 7.2 by the ^{1}H NMR measurement from the comparison

* Corresponding authors. E-mail: kmayumi@molle.k.u-tokyo.ac.jp (K.M.); kohzo@molle.k.u-tokyo.ac.jp (K.I.).
† Graduate School of Frontier Sciences.
‡ Institute for Solid State Physics.

10.1021/ma801021g CCC: $40.75
Published on Web 08/05/2008

Table 1. Molecular Weights, Mass Densities, Molecular Volumes, and Scattering Length Densities of the Polymers and Solvent Used in This Study

sample	molecular weight (g mol^{-1})	mass density d (g mL^{-1})	molecular volume V_w (cm^3 mol^{-1})	scattering length density ρ (10^{10} cm^{-2})
PEG	3.5×10^4	1.14	3.1×10^4	0.65
H-PR	1.8×10^5	1.35	1.3×10^5	1.2
DMSO-d_6	84	1.19	71	5.3

between the CH_3 protons of the hydroxypropyl groups and the other ones.

In the SANS experiments, we used DMSO-d_6 as the solvent. Table 1 shows the characteristics of PEG, H-PR, and DMSO-d_6: their molecular weights, mass densities, molecular volumes, and scattering length densities. The mass densities were evaluated by using a DMA 5000 density meter (Anton Paar, Graz, Austria). The molecular weights of H-PR were estimated from the average numbers of CDs per PEG chain and hydroxypropyl groups per CD, which were determined by the ^{1}H NMR results.

In order to compare between H-PR and the template PEG, H-PR and PEG solutions in DMSO-d_6 were prepared in the same molar concentration regime. We performed the SANS experiments of PEG solutions at the polymer concentrations of 0.17, 0.34, 0.85, and 1.7 μmol/mL (6.0, 12, 30, and 59 mg/mL) and those of H-PR solutions at 0.067, 0.33, and 0.69 μmol/mL (12, 59, and 123 mg/mL). The molar concentrations were calculated by using the molecular weight given in Table 1.

2.2. Small-Angle Neutron Scattering. Small-angle neutron scattering (SANS) experiments were performed using the SANS-U spectrometer of the Institute for Solid State Physics, the University of Tokyo, located at the JRR-3M research reactor of Japan Atomic Energy Agency in Tokai, Japan.[31] The neutron wavelength λ was 7.0 Å with $\Delta\lambda/\lambda = 10\%$ full width at half-maximum, and the sample-to-detector distances were 4 and 1 m. This setup resulted in an experimental Q range of 0.01−0.3 Å^{-1}. Here, Q is the magnitude of the scattering vector:

$$Q = \frac{4\pi}{\lambda} \sin\left(\frac{\theta}{2}\right) \tag{1}$$

where θ is the scattering angle. The scattered neutrons were collected with a two-dimensional detector (model 2660N, Ordela), and then the necessary corrections were made, such as air scattering and cell scattering subtraction. After these corrections, the scattered intensity was normalized to the absolute intensity in terms of the scattering intensity from a standard sample. Data reduction was carried out by the circular averaging of the two-dimensional intensity data, followed by the incoherent scattering subtraction.[32] The temperature of the sample was regulated to be 25 °C by a water-circulating bath controlled with a Neslab RTE-111 thermocontroller with a precision of ±0.1 °C.

3. Results and Discussion

3.1. Ornstein−Zernike Equation. Figure 1 shows the scattering functions of PEG and H-PR solutions in DMSO-d_6 at various concentrations. The scattering function $I(Q)$ of polymer chains in a semidilute solution is usually analyzed by using the Ornstein−Zernike (OZ) equation[33]

$$I(Q) = \frac{I(0)}{1 + Q^2\xi^2} \tag{2}$$

where ξ is the correlation length. The solid curves in Figure 1 show the best-fitting results of eq 2. It was clear that the scattering functions for PEG in DMSO-d_6 were well fitted with eq 2. Figure 2 shows the concentration dependence of $I(0)$ for PEG in DMSO-d_6. The $I(0)$ of PEG increased proportionally with polymer concentration c_p below 0.34 μmol/mL (12 mg/mL); however, it deviated from the proportional increase above

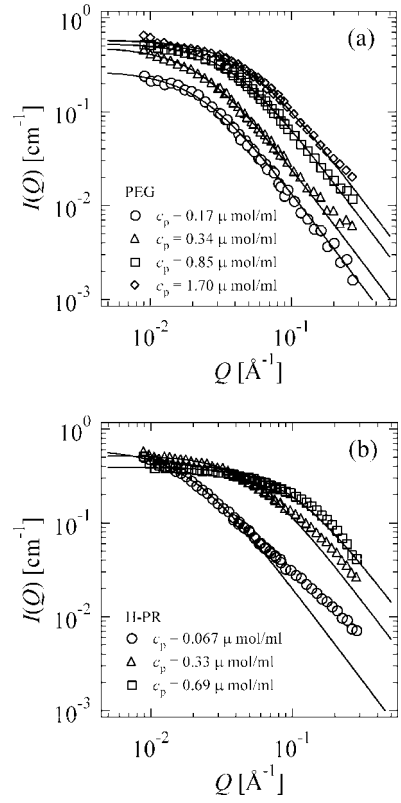

Figure 1. Scattering intensity vs scattering vector Q for (a) PEG solutions and (b) H-PR solutions. The solid curves represent the fitting results with the Ornstein−Zernike equation.

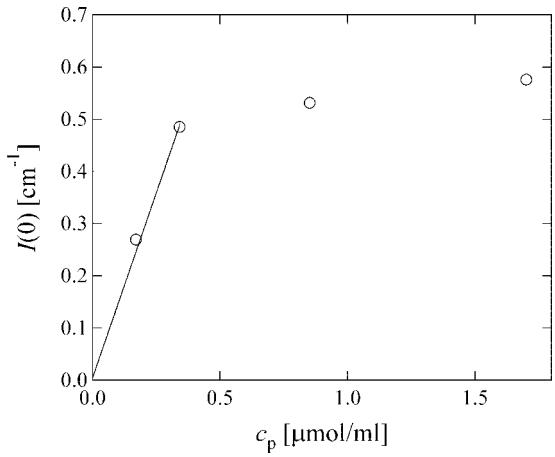

Figure 2. Plot of $I(0)$ as a function of polymer concentration c_p for PEG. The solid line shows that $I(0)$ for PEG in the low-concentration regime is proportional to c_p.

the concentration of 0.34 μmol/mL due to the excluded volume effect.[34] This suggested that the crossover or overlap concentration c^* was around 0.34 μmol/mL. This suggestion was supported by the double-logarithmic plot of ξ against c_p given in Figure 3. It was observed that ξ was independent of c_p in the dilute regime and decreased with increasing c_p above 0.34 μmol/mL. On the other hand, the scattering functions for H-PR were not fitted well with eq 2, especially in the high-Q range, as clearly shown in Figure 1b. This was mainly because the persistence length l_p and diameter R of H-PR were considerably larger than those of the template PEG due to the inclusion complex formation with CDs.[24] The difference in l_p and R between PEG and H-PR in the nanometer scale should appear definitely in the high-Q range. Moreover, the $I(0)$ of H-PR decreased drastically with increasing c_p, as shown in Figure 1b.

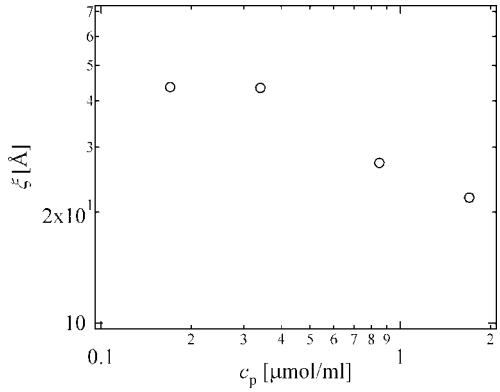

Figure 3. Double-logarithmic plot of ξ as a function of c_p for PEG.

Since the OZ function is derived from the mean-field theory, it is difficult to be applied to the semidilute polymer solution near c^* due to the large density fluctuations. On the other hand, it is to be noted that the analysis using the OZ equation can provide a rough classification of polymer solutions, i.e., whether the solution is in the dilute, semidilute, or concentrated region, as mentioned above.

3.2. Generalized Zimm Plot. In order to study the molecular conformation and interaction of PEG and H-PR in DMSO-d_6, we employed the generalized Zimm plot, which has been applied to semidilute as well as dilute solutions,[26] given by

$$I(Q) = \frac{(\rho_P - \rho_S)^2}{N_A} \frac{\Phi(1-\Phi)}{1/(V_w P(Q)) + 2A_{2,app}\Phi} \tag{3}$$

Here, N_A is the Avogadro constant, $\rho_{P/S}$ the scattering length density of the polymer/solvent, Φ the volume fraction of the polymer, V_w the weight-average molecular volume, $P(Q)$ the form factor that describes the molecular architecture of the polymer, and $A_{2,app}$ the apparent second virial coefficient. $A_{2,app}$ can be expanded in the powers of c_p as follows[35]

$$A_{2,app} = A_2 + \frac{3}{2}A_3 c_p + \cdots \tag{4}$$

where A_2 and A_3 are the second and third virial coefficients, respectively. The generalized Zimm analysis is based on the single-contact approximation, which is more valid in the concentration regime from the dilute regime to the semidilute regime around c^* than the mean-field approximation.

We adopted the scattering function of a wormlike chain as the form factor $P(Q)$, which would represent the various possible chain conformations from flexible chains like PEG to more rigid ones like PR. Yoshizaki and Yamakawa derived the scattering function of the wormlike chains[36] to be

$$P_{KP}(Q) = P_0(Q;L)\,\Gamma(Q;L) \tag{5}$$

where L is the length of the polymer chain. In this case, L was evaluated to be 2.8×10^3 Å from the monomer length of PEG, 3.5 Å,[37] and $\Gamma(Q;L)$ in eq 5 is the sum of additive factors calculated by Yoshizaki and Yamakawa.[36] $P_0(Q;L)$ is given by

$$P_0(Q;L) = [1-\chi(Q;L)]P_{Debye}(Q;L) + \chi(Q;L)\,P_{rod}(Q;L) \tag{6}$$

where $P_{Debye}(Q;L)$ is the Debye scattering function for a random coil given by

$$P_{Debye}(Q;L) = 2u^{-2}(e^{-u} + u - 1) \tag{7}$$

with $u = R_g^2 Q^2$. Here R_g is the mean-square radius of gyration for the wormlike chain, derived by Benoit and Doty[38] as

$$R_g^2 = \frac{Ll_P}{3} - l_P^2 + \frac{2l_P^3}{L} - \frac{2l_P^4}{L^2}(1 - \exp(-L/l_P)) \tag{8}$$

On the other hand, P_{rod} in eq 6 represents the scattering function for a infinitely thin rod with a length L, written as

$$P_{rod}(Q;L) = \frac{2}{QL}Si(QL) - \sin^2\left(\frac{QL}{2}\right) \tag{9}$$

where $Si(x)$ is the sine integral. Moreover, the factor $\chi(Q;L)$ in eq 6 is given by

$$\chi = \exp(-(\pi R_g^2 Q/2L)^{-5}) \tag{10}$$

When $P(Q)$ in eq 3 was given by the wormlike chain model, we had two adjustable parameters, $A_{2,app}$ and l_p, and the other parameters were fixed for the analysis of the scattering data. $A_{2,app}$ and l_p determined the initial scattering intensity $I(0)$ and the crossover Q from a Guinier regime to a power-law regime of the scattering curve, respectively. The scattering functions for PEG solutions were fitted well with eqs 3 and 5; however, those for H-PR deviated from the wormlike chain model at high Q, as shown by the dashed lines in Figure 4b. This was because H-PR had a larger diameter than the PEG chain due to the inclusion of CD molecules with the radius of about 7 Å.[39] Therefore, for fitting the experimental data of H-PR, we used the scattering function for the cylinder $P_{Cyl}(Q;L;R)$ instead of P_{rod} in eq 6

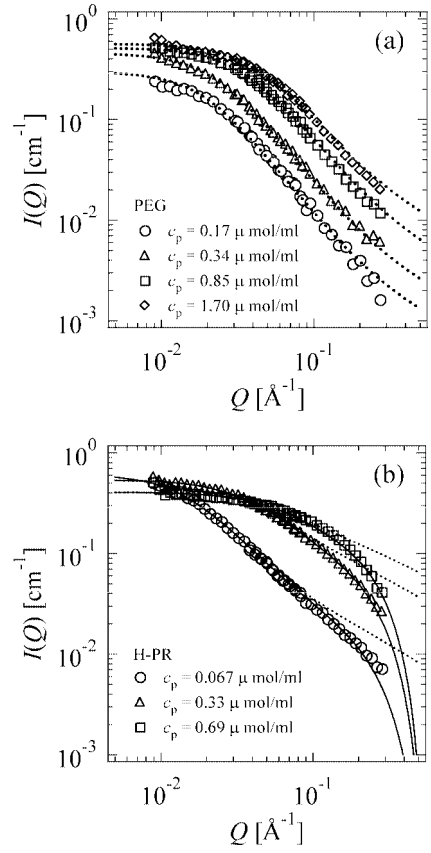

Figure 4. Fitting results of the experimental data to the generalized Zimm plot. The dashed and solid curves are derived from eq 3 with the form factor for the wormlike chain model and for the modified wormlike chain model taking account of the polymer radius, respectively.

$$P_{cyl}(Q;L;R) = \int_0^{\pi/2} \left\{ \frac{2J_1(QR\sin\alpha)}{QR\sin\alpha} \frac{\mathrm{Sin}\left(\frac{QL}{2}\cos\alpha\right)}{\frac{QL}{2}\cos\alpha} \right\}^2 \sin\alpha\, d\alpha \quad (11)$$

where R is the radius of the cylinder, $J_1(x)$ is the first-order cylindrical Bessel function, and $\int_0^{\pi/2} \sin\alpha\, d\alpha$ in eq 11 represents the random orientation of the cylinders. R influences the high-Q behavior of the scattering function as clearly shown in Figure 5. When R is zero, the $I(Q)$ in the high-Q regime behaves as $I(Q) \sim Q^{-1}$, corresponding to the form factor of the rod with the persistence length l_p. As R increases, $I(Q)$ crosses over from the scattering function of the rod in the lower Q range to that of the disk with the radius R in the higher Q range, deviating from $I(Q) \sim Q^{-1}$. The scattering curves of H-PR were well described by this modified wormlike chain model with R fixed at the radius of CD, 7 Å, as shown by the solid curves in Figure 4b. The fitting parameters obtained are summarized in Table 2.

3.3. Characteristic Features of H-PR. Figure 6 shows the comparison of $A_{2,app}$ between PEG and H-PR in DMSO-d_6. With eq 4, A_2 and A_3 are evaluated from the intercept and the initial slope of a plot of $A_{2,app}$ against the polymer concentration c_p. Whereas $A_{2,app}$ in the PEG solutions was almost independent of c_p, that in the H-PR solutions increased with c_p in the same molar concentration regime, corresponding to the concentration dependence of $I(0)$ shown in Figure 1b. This indicates that A_3 of H-PR was larger than that of PEG, which is consistent with the experimental results that A_3 increases with molecular weight.[40] Incidentally, H-PR including many CDs had the molecular weight of 1.8×10^5, which was considerably larger than that of PEG before complexation with CDs.

Figure 7 shows that the persistence length l_p of H-PR was also considerably longer than that of PEG. The inclusion complex formation with CDs stretched the PEG chain, as

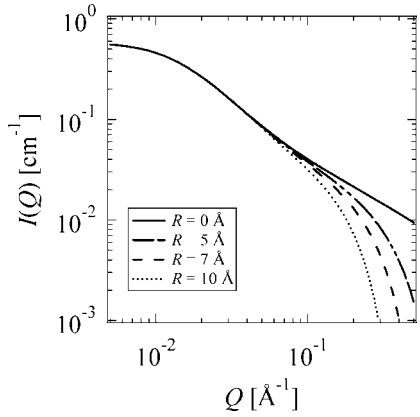

Figure 5. Scattering curves calculated from eq 3 with the modified wormlike chain model. The radius R was varied from 0 to 10 Å with the other parameters fixed: $\rho_p = 1.2$, $\rho_s = 5.3$, $\Phi = 0.01$, $V_w = 1.3 \times 10^5$ cm^3 mol^{-1}, $L = 2.8 \times 10^3$ Å, $l_p = 50$ Å, and $A_{2,app} = 0.002$ cm^3 mol g^{-2}.

Table 2. Summary of the Fitting Results with the Generalized Zimm Plot for PEG and H-PR in DMSO-d_6

sample	concn (μmol mL^{-1}, mg mL^{-1})	$A_{2,app}$ (10^{-3} cm^3 mol g^{-2})	l_p (Å)
PEG/DMSO-d_6	0.17, 6.0	2.8	11
	0.34, 12	2.3	11
	0.85, 30	2.7	9
	1.7, 59	2.7	11
H-PR/DMSO-d_6	0.067, 12	1.9	44
	0.33, 59	2.4	33
	0.69, 123	3.1	30

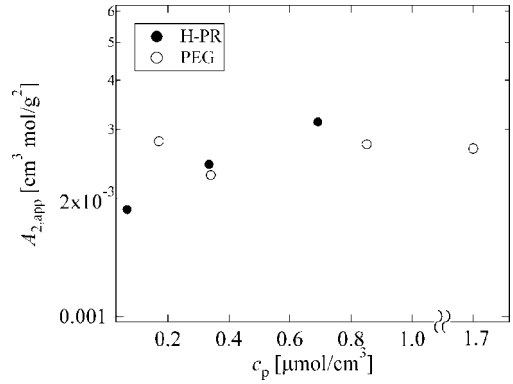

Figure 6. Plot of $A_{2,app}$ as a function of c_p for H-PR (●) and PEG (○).

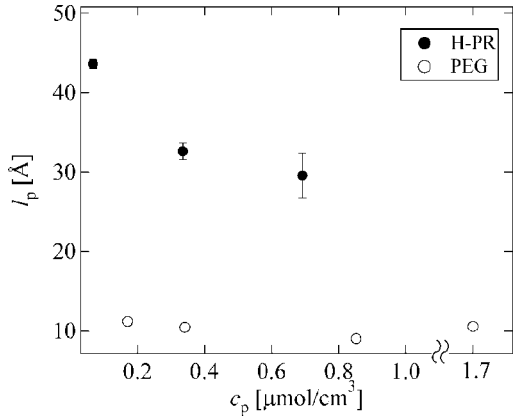

Figure 7. Plot of l_p as a function of c_p for H-PR (●) and PEG (○).

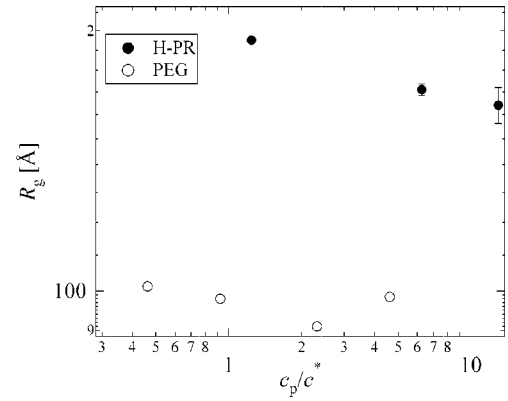

Figure 8. Double-logarithmic plot of R_g calculated from eq 8 as a function of c_p/c^*.

reported in the previous works.[24] In addition, the concentration dependence of l_p of H-PR differed from that of the l_p of PEG: l_p of H-PR decreased with an increase of c_p from 0.05 to 1 μmol/mL, while that of PEG remained almost constant in the same molar concentration range. The decrease in l_p with increasing c_p in H-PR may be due to the suppression of the mobility of CD in H-PR caused by increasing c_p. The free and rapid sliding of CDs along PEG should extend H-PR to rigid conformation, leading to an increase in l_p. On the other hand, if CDs are fixed at PEG without free sliding in H-PR, l_p ought to decrease to an average value between PEG and CD, depending on the filling ratio. Consequently, the peculiar concentration dependence of l_p decreasing with increasing c_p in H-PR supported the conclusion that the mobility of CDs in H-PR was suppressed by the increasing c_p.

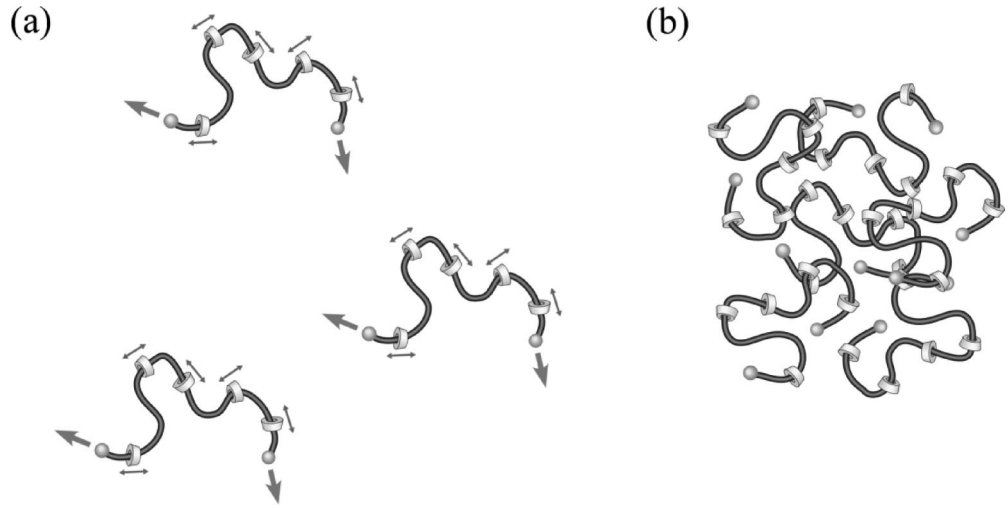

Figure 9. Schematic diagram of PR including CDs sparsely (a) in dilute solution and (b) in semidilute solution. The diffusive force from CDs confined in PR stretches the PEG chain of PR in the dilute regime, while it disappears since CDs are dispersed homogeneously in the semidilute solution.

We calculated the radius of gyration R_g from the persistence length l_p by using eq 8. Figure 8 is a double-logarithmic plot of R_g for PEG and H-PR as a function of c_p/c^*, where the overlap concentration c^* is defined by

$$c^* = \frac{M_w/N_A}{(4/3)\pi R_g^3} \tag{12}$$

If the R_gs of H-PR and PEG at the lowest concentration (12 mg/mL for H-PR and 6.0 mg/mL for PEG) could be regarded as the coiled radius in a dilute solution, the overlap concentrations would be $c^*_{\text{H-PR}} = 10$ mg/mL for H-PR, which was almost equal to the lowest concentration (12 mg/mL) of H-PR, and $c^*_{\text{PEG}} = 13$ mg/mL for PEG. Figure 8 indicated that the radius R_g of PEG remained unchanged in the semidilute regime near c^* ($1 < c/c^* < 4$), while R_g of H-PR decreased continuously with increasing c_p for $c/c^* > 1$. This unique concentration dependence of R_g for H-PR, which was different from that of PEG, comes from that of l_p and hence may be attributed to some molecular interaction, such as the steric constraint between CDs, reducing the mobility of CDs in H-PR as mentioned before. Incidentally, the mobility of CDs in PR should inherently yield the dependence of the polymer conformation on c_p from the entropic point of view. In the dilute regime, CDs localized within the PEG chains by bulky end-caps, as illustrated in Figure 9a, tend to diffuse to the outer region, away from H-PR, by thermal agitation in order to reduce the concentration difference of CDs between the inside and the outside of R_g of H-PR if they move freely along PEG in H-PR. The sliding behavior of CDs trapped on PEG chains by bulky end-caps would stretch the PEG chains, as the gas pressure in a piston expands the volume. On the other hand, CDs are distributed homogeneously in the semidilute solution, as shown schematically in Figure 9b. As a result, a drastic decrease in R_g would be caused by not only the screening of excluded volume effects but also vanishing the internal pressure of CDs in H-PR mentioned above. This phenomenon seems analogous to the conformational change in polyelectrolytes in solutions, where the PEG chain and CDs trapped on PEG topologically by the end-capping with bulky groups correspond to a polyion and counterions bound to the polyion by the Coulombic interaction, respectively.

4. Conclusion

Small-angle neutron scattering (SANS) experiments were carried out to investigate the conformation of hydroxypropylated polyrotaxane (H-PR), consisting of hydroxypropylated α-cyclodextrins (CDs) and poly(ethylene glycol) (PEG), in deuterated dimethyl sulfoxide (DMSO-d_6) in the semidilute regime near the overlap concentration c^*, and compared it to that of the template PEG. The following facts were disclosed.

(1) The scattering functions of H-PR deviated from the Ornstein−Zernike function in the high-Q range, while those of PEG were fitted with it. The high-Q behavior in the scattering functions of H-PR reflected the local molecular conformation such as the persistence length l_p and radius R of H-PR. The difference in the scattering functions between H-PR and PEG in the high-Q range indicated that H-PR had l_p and R that were considerably larger than those of the template PEG chain due to the threading of CDs on the PEG in H-PR.

(2) The generalized Zimm plot with the form factor derived from a wormlike chain model provided information on the molecular conformation and interaction in the semidilute solutions such as R, l_p, and the apparent second virial coefficient $A_{2,\text{app}}$. As a result, the following findings were obtained. First, the scattering functions of H-PR were fitted well with R fixed at the radius of CD, 7 Å. Second, the $A_{2,\text{app}}$ of H-PR increased with c_p while that of PEG remained unchanged in the same molar concentration regime. This was ascribed to the third virial coefficient A_3 of H-PR that was considerably larger than that of PEG since H-PR has a greater molecular weight than PEG. Finally, the l_p and the radius of gyration R_g, estimated from l_p, of H-PR decreased with increasing c_p in the semidilute regime near c^*, whereas those of PEG remained almost constant. This unusual concentration dependence of polymer conformation for H-PR may suggest that CDs in H-PR could slide freely and rapidly on the whole range of PEG chains in the neighborhood of c^*, but their mobility was suppressed as c_p increased by some molecular interaction among CDs such as the steric constraint between CDs. The experimental results of the molecular conformation and interaction of H-PR were quite important for us to understand the various properties of the polymeric materials made from PR such as the slide ring gels.

Acknowledgment. This work was partially supported by the Ministry of Education, Science, Sports and Culture, Japan (Grant-in-Aid for Scientific Research on Priority Areas, 2006-2010, No. 18068004), and Grant-in-Aid for Scientific Research ((S), 2008−2012, No. 20221005). The SANS experiment was performed with the approval of Institute for Solid State Physics, The University of

Tokyo (Proposal No. 7607), at Japan Atomic Energy Agency, Tokai, Japan.

References and Notes

(1) Philp, D.; Stoddart, J. F. *Angew. Chem., Int. Ed.* **1996**, *35*, 1155.
(2) Wenz, G. *Angew. Chem., Int. Ed.* **1994**, *33*, 803.
(3) Harada, A.; Hashidzume, A.; Takashima, Y. *Adv. Polym. Sci.* **2006**, *201*, 1.
(4) Harada, A.; Li, J.; Kamachi, M. *Nature (London)* **1992**, *356*, 325.
(5) Harada, A.; Li, J.; Nakamitsu, T.; Kamachi, M. *J. Org. Chem.* **1993**, *58*, 7524.
(6) Huang, F.; Gibson, H. W. *Prog. Polym. Sci.* **2005**, *30*, 982.
(7) Wenz, G.; Han, B. H.; Muller, A. *Chem. Rev.* **2006**, *106*, 782.
(8) Araki, J.; Ito, K. *Soft Matter* **2007**, *3*, 1456.
(9) Loethen, S.; Kim, J. M.; Thompson, D. H. *Polym. Rev.* **2007**, *47*, 383.
(10) Harada, A.; Li, J.; Kamachi, M. *Nature (London)* **1993**, *364*, 516.
(11) Cacialli, F.; Wilson, J. S.; Michels, J. J.; Daniel, C.; Silva, C.; Friend, R. H.; Severin, N.; Samori, P.; Rabe, J. P.; O'Connell, M. J.; Taylor, P. N.; Anderson, H. L. *Nat. Mater.* **2002**, *1*, 160.
(12) Shimomura, T.; Akai, T.; Abe, T.; Ito, K. *J. Chem. Phys.* **2002**, *116*, 1753.
(13) Ooya, T.; Yui, N. *J. Controlled Release* **1999**, *58*, 251.
(14) Ooya, T.; Eguchi, N.; Yui, N. *J. Am. Chem. Soc.* **2003**, *125*, 13016.
(15) Okumura, Y.; Ito, K. *Adv. Mater.* **2001**, *13*, 485.
(16) Ito, K. *Polym. J.* **2007**, *39*, 489.
(17) Karino, T.; Okumura, Y.; Zhao, C. M.; Kataoka, T.; Ito, K.; Shibayama, M. *Macromolecules* **2005**, *38*, 6161.
(18) Karino, T.; Shibayama, M.; Ito, K. *Physica B* **2006**, *385*−*386*, 692.
(19) Shinohara, Y.; Kayashima, K.; Okumura, Y.; Zhao, C.; Ito, K.; Amemiya, Y. *Macromolecules* **2006**, *39*, 7386.
(20) Zhao, T.; Beckham, H. W. *Macromolecules* **2003**, *36*, 9859.
(21) Ceccato, M.; Nostro, P. L.; Rossi, C.; Bonechi, C.; Donati, A.; Baglioni, P. *J. Phys. Chem. B* **1997**, *101*, 5094.
(22) Zhao, C.; Domon, Y.; Okumura, Y.; Okabe, S.; Shibayama, M.; Ito, K. *J. Phys.: Condens. Matter* **2005**, *17*, S2841. 2005.
(23) Karino, T.; Okumura, Y.; Ito, K.; Shibayama, M. *Macromolecules* **2004**, *37*, 6177.
(24) Fleury, G.; Brochon, C.; Schlatter, G.; Bonnet, G.; Lapp, A.; Hadziioannou, G. *Soft Matter* **2005**, *1*, 378.
(25) Jarroux, N.; Guegan, P.; Cheradame, H.; Auvray, L. *J. Phys. Chem. B* **2005**, *109*, 23816.
(26) Stellbrink, J.; Willner, L.; Jucknischke, O.; Richter, D.; Lindner, P.; Fetters, L. J.; Huang, S. *Macromolecules* **1998**, *31*, 4189.
(27) Araki, J.; Ito, K. *J. Polym. Sci., Part A: Polym. Chem.* **2006**, *44*, 6312.
(28) Ooya, T.; Yui, N. *Macromol. Chem. Phys.* **1998**, *199*, 2311.
(29) Araki, J.; Zhao, C.; Ito, K. *Macromolecules* **2005**, *38*, 7524.
(30) Harada, A.; Li, J.; Kamachi, M. *Macromolecules* **1993**, *26*, 5698.
(31) Okabe, S.; Karino, T.; Nagao, M.; Watanabe, S.; Shibayama, M. *Nucl. Instrum. Methods A* **2007**, *572*, 853.
(32) Shibayama, M.; Nagao, M.; Okabe, S.; Karino, T. *J. Phys. Soc. Jpn.* **2005**, *74*, 2728.
(33) de Gennes, P. G. *Scaling Concepts in Polymer Physics*; Cornell University Press: Ithaca, NY, 1979.
(34) Daoud, M.; Cotton, J. P.; Farnoux, B.; Jannink, G.; Sarma, G.; Benoit, H.; Duplessix, R.; Picot, C.; de Gennes, P. G. *Macromolecules* **1975**, *8*, 804.
(35) Yamakawa, H. *Modern Theory of Polymer Solutions*; Harper & Row: New York, 1971.
(36) Yoshizaki, T.; Yamakawa, H. *Macromolecules* **1980**, *13*, 1518.
(37) Hansen, P. L.; Cohen, J. A.; Podfornik, R.; Parsegian, V. A. *Biophys. J.* **2003**, *84*, 350.
(38) Benoit, H.; Doty, P. *J. Phys. Chem.* **1953**, *57*, 958.
(39) Lichtenthaler, F. W.; Immel, S. *Tetrahedron: Asymmetry* **1994**, *5*, 2045.
(40) Sato, T.; Norisuye, T.; Fujita, H. *J. Polym. Sci, Part B: Polym. Phys.* **1987**, *25*, 1.

MA801021G